Synthetic, X-ray Structure, Electron Paramagnetic Resonance, and Magnetic Studies of the Manganese(II) Complex of 1-Thia-4,7-diazacyclononane ([9]aneN$_2$S)

Lawrence R. Gahan,[1a] Vincent A. Grillo,[1a] Trevor W. Hambley,[1b] Graeme R. Hanson,*[,1c] Clifford J. Hawkins,[1a,d] Emma M. Proudfoot,[1b] Boujemaa Moubaraki,[1e] Keith S. Murray,[1e] and Deming Wang[1c]

Department of Chemistry and Centre for Magnetic Resonance, The University of Queensland, Brisbane, QLD 4072, Australia, The School of Chemistry, The University of Sydney, Sydney, NSW 2006, Australia, and Chemistry Department, Monash University, Clayton, Victoria 3168, Australia

Received May 4, 1995[⊗]

Reaction of manganese(II) perchlorate hexahydrate with a methanol solution of 1-thia-4,7-diazacyclononane ([9]aneN$_2$S) resulted in the isolation of the manganese(II) complex [Mn([9]aneN$_2$S)$_2$](ClO$_4$)$_2$. The X-ray structure of this complex is reported: crystal system orthorhombic, space group *Pbam*, No. 55, $a = 7.937(2)$ Å, $b = 8.811(2)$ Å, $c = 15.531(3)$ Å, $Z = 2$, $R = 0.0579$. The complex is high spin ($S = {}^5/_2$) with an effective magnetic moment (μ_{eff}) 5.82 μ_B at 298 K and 5.65 μ_B at 4.2 K. Computer simulation of the Q-band EPR spectrum of [Mn([9]aneN$_2$S)$_2$](ClO$_4$)$_2$ yields $g = 1.99 \pm 0.01$, $|D| = 0.19 \pm 0.005$ cm^{-1}, and $E/D = 0.04 \pm 0.02$. For the analogous hexaamine complex [Mn([9]aneN$_3$)$_2$](ClO$_4$)$_2$ ([9]aneN$_3$ = 1,4,7-triazacyclononane) analysis of the EPR spectra produced the following values: $g = 1.98 \pm 0.01$, $|D| = 0.09 \pm 0.003$ cm^{-1}, and $E/D = 0.1 \pm 0.01$. The spin Hamiltonian parameters for [Mn([9]aneN$_2$S)$_2$](ClO$_4$)$_2$ derived from the EPR spectra produced a good fit to the magnetic susceptibility data.

Introduction

Interest in the coordination chemistry of manganese has been dominated by the pursuit of models for the molecular structure, electronic structure, and reactivity of the manganese sites in biological systems.[2−7] More recently, the potential application of manganese complexes for clean and efficient low temperature bleaching has also been explored.[8]

In the majority of studies, the biological model complexes involve oxygen or nitrogen donor ligands, donors associated with the classical coordination chemistry of manganese in oxidation states II−VII. Nitrogen donor ligands, particularly the macrocyclic cyclononane ligands 1,4,7-triazacyclononane ([9]aneN$_3$) and 1,4,7-trimethyl-1,4,7-triazacyclonone (Me$_3$[9]aneN$_3$), have been central in the studies of the synthesis of mononuclear and dinuclear complexes of manganese, and the modeling of biological roles of this metal.[9−23] In addition, the chemistry of manganese(II) with the ligand 1-oxa-4,7-diazacyclononane ([9]aneN$_2$O) has recently been explored.[24]

While examples of manganese interaction with these ligands have been important in the development of the understanding of the biological roles of the metal, the chemistry of manganese with other donors has not been as completely developed. For example, the role of the manganese−thioether interaction in coordination chemistry and in biological systems has not been completely elucidated. The first structurally characterized example of a Mn(II)−thioether bond in the complex [Mn(Me2L)], (Me2L = [1,2-bis((*o*-(1-methyl-1-oxidotriazen-3-yl)-phenyl)thio)ethanato-*N*^{3},*S*,*O*]), was reported recently.[25] There

* Author to whom correspondence should be addressed.

⊗ Abstract published in *Advance ACS Abstracts,* January 15, 1996.

(1) (a) Department of Chemistry, The University of Queensland. (b) The University of Sydney. (c) Centre for Magnetic Resonance, The University of Queensland. (d) Present address: ICT Diagnostics, P. O. Box 228, Brookvale, NSW, 2100, Australia. (e) Chemistry Department, Monash University.
(2) Que, L., Jr.; True, A. E. *Prog. Inorg. Chem.* **1990,** *38,* 97.
(3) Wieghardt, K. *Angew. Chem., Int. Ed. Engl.* **1989,** *28,* 1153.
(4) Christou, G. *Acc. Chem. Res.* **1989,** *22,* 328.
(5) Thorpe, H. H.; Brudwig, G. W. *New J. Chem.* **1991,** *15,* 479.
(6) Brudvig, G. W. *ACS Symp. Ser.* **1988,** *372,* 221.
(7) Christou, G.; Vincent, J. B. *ACS Symp. Ser.* **1988,** *372,* 238.
(8) Haǵe, R.; Iburg, J. E.; Kerschner, J.; Koek, J. H.; Lempers, E. L. M.; Martens, R. J.; Racheria, U. S.; Russell, S. W.; Swarthoff, T.; van Vliet, M. R. P.; Warnaar, J. B.; van der Wolf, L.; Krijnen, B. *Nature* **1994,** *369,* 637.
(9) Wieghardt, K.; Schmidt, W.; Küppers, H.-J. *Inorg. Chem.* **1983,** *22,* 2953.
(10) Wieghardt, K.; Tolksdorf, I.; Herrmann, W. *Inorg. Chem.* **1985,** *24,* 1230.
(11) Wieghardt, K.; Bossek, U.; Gebert, W. *Angew. Chem., Int. Ed. Engl.* **1983,** *22,* 328.
(12) Wieghardt, K.; Bossek, U.; Gebert, W. *Angew. Chem., Int. Ed. Engl.* **1986,** *25,* 1030.
(13) Bossek, U.; Wieghardt, K.; Nuber, B.; Weiss, J. *Inorg. Chim. Acta* **1989,** *165,* 123.
(14) Wieghardt, K.; Bossek, U.; Nuber, B.; Weiss, J.; Bonvoisin, J.; Corbella, M.; Vitols, S. E.; Girerd, J. J. *J. Am. Chem. Soc.* **1988,** *110,* 7398.
(15) Wieghardt, K.; Bossek, U.; Ventur, D.; Wiess, J. *J. Chem. Soc., Chem. Commun.* **1985,** 347.
(16) Wieghardt, K.; Bossek, U.; Zsolnai, L.; Huttner, G.; Blondin, G.; Girerd, J.-J.; Babonneau, F. J. *Chem. Soc., Chem. Commun.* **1987,** 651.
(17) Wieghardt, K.; Bossek, U.; Nuber, B.; Weiss, J. *Inorg. Chim. Acta* **1987,** *126,* 39.
(18) Bossek, U.; Weyhermüller, T.; Wieghardt, K.; Nuber, B.; Wiess, J. *J. Am. Chem. Soc.* **1990,** *112,* 6387.
(19) Hotzelmann, R.; Wieghardt, K.; Flörke, U.; Haupt, H.-J.; Weatherburn, D. C.; Bonvoisin, J.; Blondin, G.; Girerd, J.-J. *J. Am. Chem. Soc.* **1992,** *114,* 1681.
(20) Chang, H.-R.; Diril, H.; Nilges, M. J.; Zhang, X.; Potenza, J. A.; Schuger, H. J.; Hendrickson, D. N.; Isied, S. S. *J. Am. Chem. Soc.* **1988,** *110,* 625.
(21) Diril, H.; Chang, H.-R.; Nilges, M. J.; Zhang, X.; Potenza, J. A.; Schuger, H. J.; Isied, S. S.; Hendrickson, D. N. *J. Am. Chem. Soc.* **1989,** *111,* 5102.
(22) Belal, A. A.; Chaudhuri, P.; Fallis, I.; Farrugia, L. J.; Hartung, R.; Macdonald, N. M.; Nuber, B.; Peacock, R. D.; Wiess, J.; Wieghardt, K. *Inorg. Chem.* **1991,** *30,* 4397.
(23) Belal, A. A.; Fallis, I.; Farrugia, L. J.; Macdonald, N. M.; Peacock, R. D. *J. Chem. Soc., Chem. Commun.* **1991,** 402.
(24) Flassbeck, C.; Wieghardt, K.; Bill, E.; Butzlaff, C.; Trautwein, A. X.; Nuber, B.; Weiss, J. *Inorg. Chem.* **1992,** *31,* 21.

0020-1669/96/1335-1039$12.00/0

are other less well-characterized examples. The binding of manganese(II) to tetrahydrothiophene has been investigated,[26] and a manganese(II)−thioether interaction has been proposed for the complex [Mn(SALDAES)] (SALDAES = 2,2′-(thiobis-(2,1-ethanediylnitrilomethylidyne)bis(phenolate)));[27] in neither case was structural verification of the interaction provided. The facially coordinating properties of the ligands [9]aneN_3 and [9]-aneN_2O, and the obviously versatile chemistry of these ligands suggested that the analogous cyclononane ligand 1-thia-4,7-diazacyclononane ([9]aneN_2S)[28] would present the possibility of enforced thioether coordination to manganese(II). This paper reports the synthesis of the complex [Mn([9]ane$N_2S)_2$]$(ClO_4)_2$ and its characterization by single-crystal structural analysis, magnetic studies, and electron paramagnetic resonance spectroscopy (EPR).[29]

Experimental Section

All manipulations were carried out under a nitrogen atmosphere using Schlenk techniques and a high vacuum line or in a VAC Vacuum Atmospheres (HE-43-2) controlled atmosphere laboratory. Methanol was dried over magnesium methoxide.

Bis(2-aminoethyl) Sulfide. To a stirred aqueous solution (1 L) of 2−bromoethylamine hydrobromide (100 g) an aqueous solution (100 mL) of NaOH (19.5 g) was added dropwise. An aqueous solution (100 mL) of $Na_2S·9H_2O$ (58.5 g) was then added dropwise over 30 min. The reaction was permitted to stir for 24 h at room temperature after which time most of the solvent was removed under reduced pressure. The white precipitate of NaBr was removed by filtration, the filtrate was made strongly basic with KOH, and the yellow oil which formed was extracted with $CHCl_3$ (4 × 100 mL). The combined $CHCl_3$ extracts were dried over Na_2SO_4 and filtered and the solvent removed under reduced pressure, resulting in a yellow oil. Krugelrohr distillation (65 °C, 0.01 mmHg) resulted in a colorless oil (17.6 g, 60%). $^{13}C[^1H]$ NMR ($CDCl_3$): δ 40.4 (CH_2NH_2), 35.0 (CH_2S).

[9]aneN_2S. The macrocyclic ligand was prepared as described previously.[28]

[Mn([9]ane$N_2S)_2$]$(ClO_4)_2$. To a stirred methanol solution (8 mL) of manganese perchlorate hexahydrate (0.31 g, 0.85 mmol) was added a methanol solution (2 mL) of [9]aneN_2S (0.30 g, 2.05 mmol) dropwise. A white precipitate formed immediately upon addition. The solution was stirred for a further 0.5 h and then filtered. The product crystallized from methanol upon standing at 4 °C (0.22 g, 48%). Anal. Calcd for $[C_{12}H_{28}N_4S_2Mn](ClO_4)_2$: C, 26.4; H, 5.2; N, 10.3. Found: C, 26.3; H, 5.3; N, 10.2.

Magnetic Studies. Magnetic susceptibility studies were performed using a Quantum Design MPMS SQUID magnetometer with an applied field of 1 T. The powdered sample was contained in a calibrated gelatin capsule which was held in the center of a soda straw fixed to the end of the sample rod. The magnetization values of the instrument were calibrated against a standard palladium sample, supplied by Quantum Design and also against chemical calibrants such as $CuSO_4·5H_2O$ and $[Ni(en)_3](S_2O_3)$ (en = ethylenediammine).

EPR Spectroscopy. Multifrequency (Q-band, ∼34 GHz and X-band, ∼9.2 GHz) EPR spectra, recorded as the first derivative of absorption, were obtained using a Bruker ESP300E EPR spectrometer. A cylindrical TE_{011} and a rectangular TE_{102} cavity were used to measure the Q- and X-band EPR spectra, respectively. Versions 3.01 and 3.02 of Bruker's esp300e software were employed for data collection. A flow through cryostat in conjunction with a Eurotherm (B-VT-2000) variable temperature controller provided temperatures of 120−140 K at the sample position in the cavity. Calibration of the microwave frequency and the magnetic field were performed with an EIP 548B microwave frequency counter and a Bruker ER-035M gaussmeter. Computer simulations were performed using SOPHE[30,31] on a SUN SPARCstation 10/30 workstation.

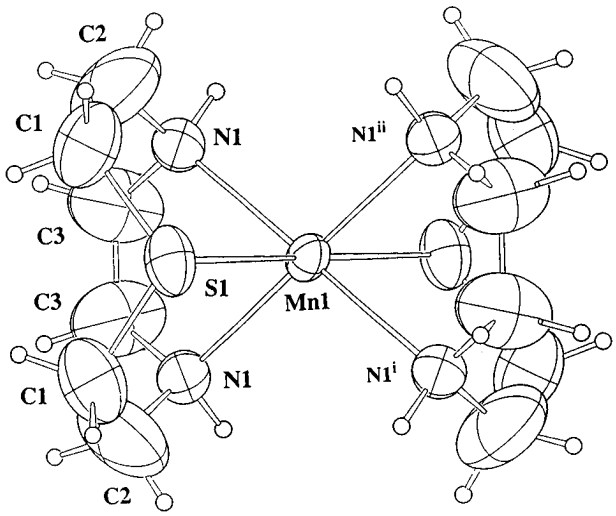

Figure 1. ORTEP plot of the cation [Mn([9]ane$N_2S)_2$]$^{2+}$ with 50% probability ellipsoids.

Table 1. Selected Crystal Data for [Mn([9]ane$N_2S)_2$]$(ClO_4)_2$

formula	$C_{12}H_{28}Cl_2N_4S_2MnO_8$	Z	2
fw	546.36	T (K)	293
space group	*Pbam* (No. 55)	ρ_{calc} (g cm^{-3})	1.676
a (Å)	7.937(2)	μ(Mo Kα) (cm^{-1})	10.11
b (Å)	8.811(2)	λ(Mo Kα) (Å)	0.710 69
c (Å)	15.531(3)	R[a]	0.058
V (Å^3)	1086.1(4)	R_w[b]	0.062

[a] $R = \sum||F_o| - |F_c||/\sum|F_o|$. [b] $R_w = (\sum w(|F_o| - |F_c|)^2/\sum w|F_o|^2)^{1/2}$, $w = 1.8/(\sigma^2(F_o) + 0.00045F_o^2)$.

X-ray Crystallography. For diffractometry the crystal (blocks, 0.08 × 0.05 × 0.12 mm) was mounted on a glass fiber with cyanoacrylate resin. Lattice parameters at 20 °C were determined by least-squares fits to the setting parameters of 25 independent reflections, measured and refined on an Enraf-Nonius CAD4-F diffractometer with a graphite monochromator. Intensity data were collected in the range $1° < \theta < 25°$. Data were reduced and Lorentz, polarization, and numerical absorption corrections were applied using the Enraf-Nonius structure determination package.[32] The structure was solved using the direct methods in SHELX-86[33] and was refined by full-matrix least-squares analysis with SHELX-76.[34] Neutral complex scattering factors were used.[35] Hydrogen atoms were included at calculated sites with fixed isotropic thermal parameters. All other atoms were refined anisotropically. Plots were drawn using ORTEP.[36] The atom numbering scheme is given in Figure 1. Selected crystal data is included in Table 1, final atomic coordinates are listed in Table 2 and listings of bond lengths and angles are given in Tables 3 and 4. The complete crystal data, non-hydrogen atom thermal parameters, hydrogen atom coordinates and thermal parameters (Tables S1−S3) are deposited as supporting information.

(25) Chakraborty, P.; Chandra, S. K.; Chakravorty, A. *Inorg. Chem.* **1993,** *32,* 5349.
(26) Rheinberger, V. M.; Sigel, H. *Naturwissenschaften* **1975,** *62,* 182.
(27) Coleman, W. M.; Boggess, R. K.; Hughes, J. W.; Taylor, L. T. *Inorg. Chem.* **1981,** *20,* 700.
(28) Gahan, L. R.; Lawrance, G. A.; Sargeson, A. M. *Aust. J. Chem.* **1982,** *35,* 1119.
(29) The International EPR Society is recommending that the acronym EPR rather than ESR be used to describe this technique.
(30) (a) Wang, D.; Hanson, G. R. *J. Magn. Reson. Ser. A* **1995**, *117*, 1. (b) Wang, D.; Hanson, G. R. Submitted for publication in *Chem. Phys. Lett.*
(31) Wang, D.; Hanson, G. R. Submitted for publication in *Appl. Magn. Res*.
(32) Enraf-Nonius Structure Determination Package. Enraf-Nonius, Delft, The Netherlands, 1985.
(33) Sheldrick, G. M. SHELXS-86. In *Crystallographic Computing 3;* Sheldrick, G. M., Krüger, C., Goddard, R., Eds.; Oxford University Press: Oxford, U.K., 1985; pp 175−189.
(34) Sheldrick, G. M.; SHELX-76, Program for Crystal Structure Determination. University of Cambridge, 1976.
(35) Cromer, D. T.; Waber, J. T. *International Tables for X-ray Crystallography;* Kynoch Press: Birmingham, U.K., 1974; Vol. 4.
(36) Johnson, C. K. *ORTEP, A Thermal Ellipsoid Plotting Program;* Oak Ridge National Laboratory: Oak Ridge, TN, 1965.

Table 2. Positional Parameters for [Mn([9]aneN$_2$S)$_2$](ClO$_4$)$_2$

atom	*x*	*y*	*z*	B_{eq}, Å^2
Mn(1)	0.0000	0.0000	0.0000	2.60
S(1)	0.0000	0.0874(5)	0.1615(2)	4.22
N(1)	−0.1764(9)	−0.1736(8)	0.0548(4)	3.79
C(1)	−0.1783(16)	−0.0265(13)	0.1941(7)	6.54
C(2)	−0.2626(18)	−0.1163(18)	0.1340(8)	9.99
C(3)	−0.0867(15)	−0.3114(12)	0.0646(11)	8.83
Cl(1)	−0.5000	−0.3269(5)	−0.1181(2)	5.69
O(1)	−0.5000	−0.2196(17)	−0.0478(7)	8.85
O(2)	−0.5000	−0.2552(19)	−0.1978(7)	9.65
O(3)	−0.6651(23)	−0.3786(19)	−0.1117(9)	14.79
O(4)	−0.5000	−0.4743(97)	−0.0983(51)	7.49
O(5)	−0.5000	−0.4984(79)	−0.1291(44)	4.99

Table 3. Bond Lengths (Å) for [Mn([9]aneN$_2$S)$_2$](ClO$_4$)$_2$

S(1)−Mn(1)	2.625(3)	N(1)−Mn(1)	2.242(7)
C(1)−S(1)	1.808(11)	C(2)−N(1)	1.497(13)
C(3)−N(1)	1.401(13)	C(2)−C(1)	1.393(15)
C(3)−C(3)	1.441(26)		

Table 4. Bond Angles (deg) for [Mn([9]aneN$_2$S)$_2$](ClO$_4$)$_2$[a]

N(1)−Mn(1)−S(1)	80.6(2)	C(1)−S(1)−Mn(1)	95.9(4)
C(2)−N(1)−Mn(1)	111.6(6)	C(3)−N(1)−Mn(1)	109.3(6)
C(3)−N(1)−C(2)	114(1)	N(1)−Mn(1)−N(1)^{i}	102.6(4)
N(1)−Mn(1)−N(1)^{ii}	77.4(4)	C(2)−C(1)−S(1)	120.4(7)
C(1)−S(1)−C(1)	103.2(8)	C(1)−C(2)−N(1)	121(1)
S(1)−Mn(1)−N(1)^{i}	90.4(2)		

[a] Symmetry: (i) *x*, −*y*, −*z*; (ii) −*x*, *y*, *z*.

Results and Discussion

Syntheses. The synthesis of the ligand [9]aneN$_2$S has been reported previously.[28] The methodology involves the cyclization reaction of the sodium salt of bis(*N*-((4-methylphenyl)sulfonyl)-2-aminoethyl) sulfide with 1,2-bis((4-methylphenyl)sulfonyl)-ethane.[37] In the present case the requisite bis(2-aminoethyl) sulfide was prepared from the reaction between sodium sulfide and (2-bromoethyl)amine. Reaction between methanol solutions of [9]aneN$_2$S and manganese perchlorate, under a nitrogen atmosphere, and subsequent crystallization of the product upon standing at 4 °C resulted in the isolation of a white crystalline material.

Discussion of Structure. The structure consists of the cation [Mn([9]aneN$_2$S)$_2$]$^{2+}$ and two perchlorate anions. A view of the complex cation is shown in Figure 1. The structural analysis indicates that all the macrocyclic donors are coordinated to the manganese(II) ion, resulting in a distorted octahedral configuration. The molecule consists of the manganese atom on a site of 2/*m* symmetry with the S atom on the mirror plane. The 2/*m* symmetry is incompatible with a normally puckered cyclononane ring and is only achieved by disorder of the chelate rings giving apparent N−C−C−N and N−C−C−S torsion angles of 0°. Attempts to resolve the disorder into separate sites were unsuccessful. The perchlorate anions are also extensively disordered. The thioether donors lie *trans*, and the secondary nitrogen donors are in the equatorial plane of the molecule.

The Mn−N bond length of 2.242(7) Å falls in the range exhibited for related high spin manganese(II) complexes, for example, the encapsulated complex [Mn(NH$_3$)$_2$sar)](NO$_3$)$_4$·H$_2$O ((NH$_3$)$_2$sar = 1,8-diammonio-3,6,10,13,16,19-hexaazabicyclo-[6.6.6]icosane) displays Mn−N bond distances ranging from 2.228(3) to 2.253(3) Å.[38] The complex [Mn([9]aneN$_3$)$_2$]$^{2+}$ has not been structurally characterized.

The Mn−S bond distance of 2.625(3) Å is similar to that reported for the complex [Mn(Me2L)], with Mn−S = 2.677-(3) Å.[25] The long Mn−S bond distance in [Mn([9]aneN$_2$S)$_2$]$^{2+}$ was predicted by Schröder *et al.* by analogy with the average Fe−S bond distance of 2.28 Å in the complex [Fe([9]-aneS$_3$)$_2$]$^{3+}$.[39] The greater Mn−S bond distance was attributed to the decrease in charge on the metal from 3+ to 2+, weakening the bond and thus labilizing the manganese−thioether interaction. Additionally, the manganese(II) ion is in the high spin state, whereas the iron(III) is low spin. Greater bond distances are usually observed for manganese(II) compounds compared to other 2+ transition metal ions due to the metal being largely ionic bonding in character.[40] This is illustrated by comparison with the iron(II) complex [Fe([9]-aneN$_2$S)$_2$](ClO$_4$)$_2$,[41] which exhibits Fe−N bond distances of 2.067(2) Å and Fe−S bond distances of 2.318(1) Å, compared to the Mn−N and Mn−S bond distances for the isovalent and isostructural complex [Mn([9]aneN$_2$S)$_2$](ClO$_4$)$_2$ of 2.242(7) and 2.625(3) Å, respectively.

Manganese−thioether interactions are known in organometallic systems where the presence of carbonyl and cyclopentadienyl groups appear to stabilize the interaction. For example, the complex [([9]aneS$_3$)Mn(CO)$_3$]$^+$ exhibited an average Mn−S bond length of 2.327 Å.[42] It was suggested that the thioether was acting as a π-acceptor, the suggestion based on an increase (0.017 Å) in the Mn−C bond length relative to the equivalent bond length in the complex *fac*-[Mn(η^1-naph)(η^2-phen)(CO)$_3$]$^+$ (naph = 1,8-naphthyridine; phen = *o*-phenanthroline) both of which are regarded as π-acceptor ligands.[43] The Mn−S bond distance in organometallic systems varies from 2.257(1) Å for a bridging thioether in the complex [(C$_6$H$_5$)Mn(CO)$_2$]$_2$S(CH$_2$)$_3$[44] to 2.404(3) Å for [(C$_6$H$_5$)$_3$PMn(CO)$_3$C(SCH$_3$)N(CH$_3$)$_2$].[45] The oxidation state of the manganese center in these systems is however, not well defined.

Magnetism. At 298 K the magnetic moment for the complex [Mn([9]aneN$_2$S)$_2$](ClO$_4$)$_2$ was 5.82 μ_B, a little lower than the spin-only value of 5.92 μ_B, and indicative of a high spin ($S = {}^5/_2$) configuration.[46] The result is consistent with that displayed by other high-spin amine complexes of manganese(II) such as [Mn(en)$_3$]Br$_2$, [Mn(sar)](ClO$_4$)$_2$, [Mn((NH$_3$)$_2$sar)](ClO$_4$)$_4$·2H$_2$O, and [Mn(Me2L)].[9,47−49]

The variable temperature (4.2−300 K) susceptibility data (Figure S1) showed that the complex [Mn([9]aneN$_2$S)$_2$](ClO$_4$)$_2$ was high spin over the whole temperature range, the moment remaining constant at 5.82 μ_B between 300 and 80 K. Further lowering of the temperature to 4.2 K produced an effective magnetic moment of 5.65 μ_B. The decrease in the moment is ascribed to second-order spin−orbit coupling and the lowering of the symmetry from octahedral, which gives rise to zero-field

(37) Richman, J. E.; Atkins, T. J. *J. Am. Chem. Soc.* **1974,** *96,* 2268.
(38) Creaser, I. I.; Engelhardt, L. M.; Harrowfield, J. MacB.; Sargeson, A. M.; Skelton, B. M.; White, A. H. *Aust. J. Chem.* **1993,** *46,* 465.
(39) Blake, A. J.; Holder, A. J.; Hyde, T. I.; Schröder, M. *J. Chem Soc., Chem. Commun.* **1989,** 1433.
(40) Chiswell, B.; McKenzie, D. E.; Lindoy, L. F. In *Comprehensive Coordination Chemistry*; Wilkinson, G., Ed.; Pergamon Books Ltd.: Oxford, U.K., 1987.
(41) Grillo, V. A. Ph.D. Thesis, The University of Queensland, 1995.
(42) Elias, H.; Schmidt, G.; Küppers, H.-J.; Saher, M.; Wieghardt, K.; Nuber, B.; Wiess, J. *Inorg. Chem.* **1989,** *28,* 3021.
(43) Bermejo, M.-J.; Ruiz, J.-I.; Solans, X.; Vinaixa, J. *Inorg. Chem.* **1988,** *27,* 4385.
(44) Bremer, G.; Boese, R.; Keddo, M.; Kruck, T. *Z. Naturforsch.* **1986,** *41,* 981.
(45) Dean, W. K.; Wetherington, J. B.; Moncrief, W. J. *Inorg. Chem.* **1976,** *15,* 1566.
(46) Figgis, B. N. *Introduction to Ligand Fields,* John Wiley & Sons, Inc.: New York, **1966**.
(47) Narain, G.; Shukla, P. *J. Indian Chem. Soc.* **1966,** *43,* 694.
(48) Watt, G. W.; Manhas, B. S. *J. Inorg. Nucl. Chem.* **1966,** *28,* 1945.
(49) Martin, L. L.; Martin, R. L.; Murray, K. S.; Sargeson, A. M. *Inorg. Chem.* **1990,** *29,* 1387.

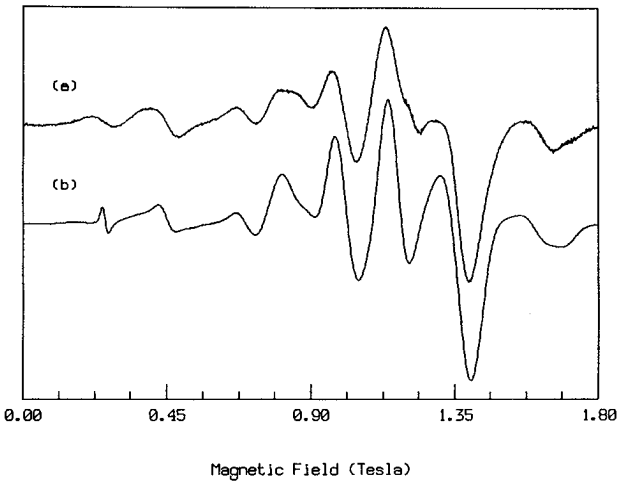

Figure 2. Q-band EPR spectra of $[Mn([9]aneN_2S)_2](ClO_4)_2$: (a) solid state spectrum, $\nu = 34.0190$ GHz at 128 K; (b) computer simulation.

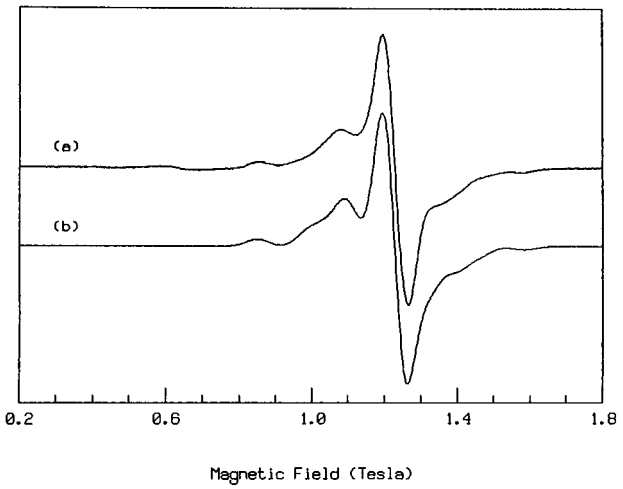

Figure 3. Q-band EPR spectra of $[Mn([9]aneN_3)_2](ClO_4)_2$: (a) solid state spectrum, $\nu = 33.9394$ GHz at 120K; (b) computer simulation.

splitting of the $^6A_{1g}$ state. The variable temperature magnetic data were analyzed taking into account the zero-field splitting contributions. Apart from small deviations in the range 20−80 K, the data fit well to an $S = {}^5/_2$ zero-field model for the ground state $^6A_{1g}$ using the spin Hamiltonian[50]

$$H = D[S_z^2 - {}^1/_3S(S+1)] + E[S_x^2 - S_y^2] + g\beta\,\mathbf{B}\cdot\mathbf{S} \quad (1)$$

where D and E, the axial and rhombic zero-field-splitting parameters, were fixed at the values obtained from EPR measurements *viz* $|D| = 0.19$ cm^{-1}, $|E| = 0.008$ cm^{-1} and the best fit g value, $g = 1.98$.

EPR Spectroscopy. The solid state Q-band EPR spectra for $[Mn([9]aneN_2S)_2](ClO_4)_2$ and $[Mn([9]aneN_3)_2](ClO_4)_2$ at 120 K are shown in Figures 2a and 3a, respectively and are richer and more resolved than the spectra obtained at X-band frequencies (Figure 4a,c, respectively). The absence of ^{55}Mn hyperfine coupling in these spectra is presumably a consequence of the very large spectral line widths.

The Q-band EPR spectrum of $[Mn([9]aneN_3)_2](ClO_4)_2$ (Figure 3a) consists of an intense resonance around $g = 2.0$ with weak resonances on both the low- and high-field sides of the main resonance, in a rather symmetric pattern. This suggests that

(50) (a) O'Connor, C. J. *Prog. Inorg. Chem.* **1982,** *29,* 203. (b) Berry, K. J.; Clark, P. E.; Murray, K. S.; Raston, C. L.; White, A. H. *Inorg. Chem.* **1983**, *22,* 3928.

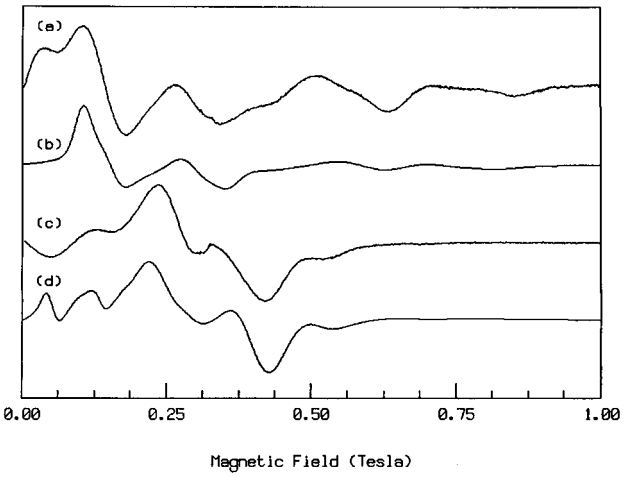

Figure 4. X-band EPR spectra of the manganese(II) cyclononane complexes: (a) solid state EPR spectrum of $[Mn([9]aneN_2S)_2](ClO_4)_2$ $\nu = 9.2997$ GHz, 120 K; (b) computer simulation of spectrum a; (c) solid state EPR spectrum of $[Mn([9]aneN_3)_2](ClO_4)_2$, $\nu = 9.2956$ GHz, 120 K; (d) computer simulation of spectrum c.

the zero-field splittings are smaller than the Q-band microwave frequency. In contrast, the Q-band EPR spectrum of $[Mn([9]aneN_2S)_2](ClO_4)_2$ (Figure 2a) is much more complicated and lacks detailed structural features, indicating that the zero-field splittings for $[Mn([9]aneN_2S)_2](ClO_4)_2$ are comparable with the Q-band microwave frequency. Clearly computer simulation of the X- and Q-band spectra is required for the quantitative determination of the spin Hamiltonian parameters.

Computer simulations were performed with a recently developed general-purpose EPR computer simulation software package SOPHE[30,31] which uses matrix diagonalization to determine the energy levels of the spin system and new methods for partitioning the unit sphere[30] and locating the resonant field positions.[31] Since the spectra of the manganese complexes (Figures 2a and 3a) lack any resolved ^{55}Mn hyperfine coupling, the spectra were simulated using the spin Hamiltonian given in eq 1 where the electron Zeeman interaction is assumed to be isotropic and only the second-order fine structure terms were considered. The simulated Q-band EPR spectra for $[Mn([9]aneN_2S)_2](ClO_4)_2$ and $[Mn([9]aneN_3)_2](ClO_4)_2$ are shown in Figures 2b and 3b, respectively. The spin Hamiltonian parameters for these simulations are as follows: $g = 1.98 \pm 0.01$, $|D| = 0.090 \pm 0.003$ cm^{-1}, and $E/D = 0.10 \pm 0.01$ ($\Delta H_x = \Delta H_y = \Delta H_z = 1000$ MHz, half-width at half-maximum) for $[Mn([9]aneN_3)_2](ClO_4)_2$; $g = 1.99 \pm 0.01$ $|D| = 0.190 \pm 0.005$ cm^{-1}, and $E/D = 0.04 \pm 0.02$ ($\Delta H_x = \Delta H_y = 1000$ MHz and $\Delta H_z = 2000$ MHz) for $[Mn([9]aneN_2S)_2](ClO_4)_2$. The larger value of D for $[Mn([9]aneN_2S)_2](ClO_4)_2$ compared to that found for $[Mn([9]aneN_3)_2](ClO_4)_2$ reflects the larger axial distortion induced by the thioether donors in the axial positions of the coordination sphere of the manganese(II) ion.

In the spectra of both complexes, significant contributions from the so-called forbidden transitions ($\Delta M_s = \pm 2, \pm 3$, etc.), which become partially allowed due to state mixing, are expected, especially for $[Mn([9]aneN_2S)_2](ClO_4)_2$. Consequently, all possible transitions among the six electronic spin states, 15 in total, were included in the simulations. The simulations showed that the two weak resonances at around 400 and 600 mT for $[Mn([9]aneN_3)_2](ClO_4)_2$ arose from the forbidden transitions, while for $[Mn([9]aneN_2S)_2](ClO_4)_2$, forbidden transitions span a much larger field range (from ∼200 up to 900 mT) because of the larger zero-field splittings.

While the simulated EPR spectra (Figures 2b and 3b) for $[Mn([9]aneN_2S)_2](ClO_4)_2$ and $[Mn([9]aneN_3)_2](ClO_4)_2$ reproduce

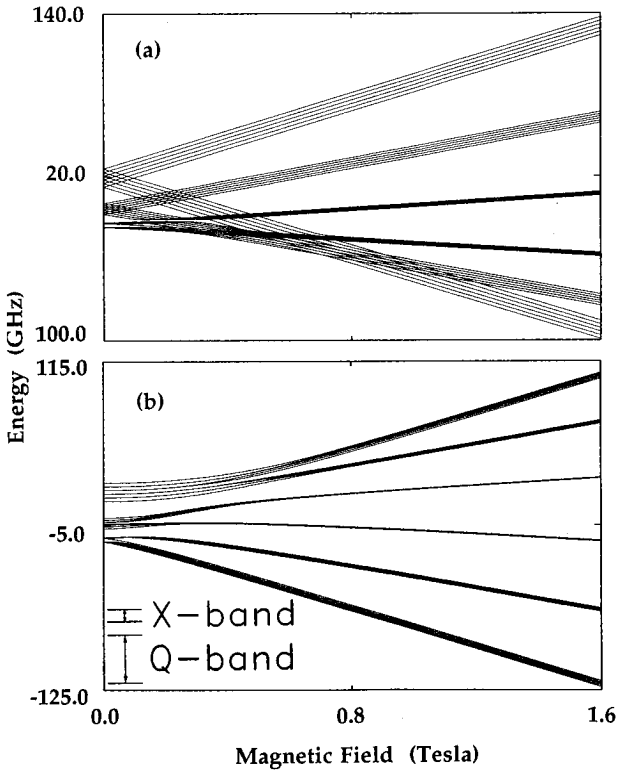

Figure 5. Energy Level Diagrams for an $S = {}^5/_2$, $I = {}^5/_2$ spin system with $g = 1.98$, $D = 0.19$ cm^{-1}, $E/D = 0.04$, $A_x = A_y = 120 \times 10^{-4}$ cm^{-1}, and $A_z = 360 \times 10^{-4}$ cm $^{-1}$: (a) B_o parallel to z; (b) B_o parallel to x.

nearly all of the resonant field positions observed experimentally, reproduction of the experimental line shape at low fields is less satisfactory in the simulated spectrum for [Mn([9]-aneN$_2$S)$_2$](ClO$_4$)$_2$ (Figure 2b). This presumably arises through the omission of ^{55}Mn hyperfine coupling in the simulation. Although no ^{55}Mn hyperfine coupling is resolved in the experimental spectra, Mn(II) complexes usually have significant ^{55}Mn hyperfine interactions. Inclusion of ^{55}Mn hyperfine coupling in the computer simulation (results not shown) significantly improved the quality of the fit in the low field region. This actually reflects the fact that a very complicated energy level diagram (energy levels vs field strength) is expected in the low field region. Representative examples of such diagrams using the values obtained from the simulation for [Mn-([9]aneN$_2$S)$_2$](ClO$_4$)$_2$ with a hyperfine term included ($A_x = A_y = 120 \times 10^{-4}$ cm^{-1}; $A_z = 360 \times 10^{-4}$ cm^{-1}) are shown in Figure 5, and the complexity in the low field region is overwhelming. Clearly, a unique determination of the ^{55}Mn hyperfine matrix from these randomly orientated frozen solution spectra is impossible.

Computer simulations were also performed for the X-band spectra (Figure 4a,c) using the same set of spin Hamiltonian parameters obtained through the simulations at Q-band and they are shown in parts b and d of Figure 4, respectively, for [Mn-([9]aneN$_2$S)$_2$](ClO$_4$)$_2$ and [Mn([9]aneN$_3$)$_2$](ClO$_4$)$_2$. Apart from the resonances close to zero field, all the major spectral features have been reproduced in the simulated spectra. Again, the less satisfactory fit shown between the measured and the simulated spectra for [Mn([9]aneN$_2$S)$_2$](ClO$_4$)$_2$ is believed to be mainly due to the omission of the ^{55}Mn hyperfine interaction. We should also mention that no attempts were made to optimize the simulation by varying the line widths as they can arise from unresolved ^{55}Mn and ligand hyperfine interactions, distributions of D and E values, and spin−lattice and spin−spin relaxation. Thus the line widths obtained from the computer simulation studies have no "direct" physical meaning.

The Q-band spectra of the complexes [Mn([9]aneN$_2$S)$_2$]-(ClO$_4$)$_2$ and [Mn([9]aneN$_3$)$_2$](ClO$_4$)$_2$ in acetonitrile−toluene (1:1) (Figure S2a,c, respectively) reveal essentially the same features as the solid state spectra (Figures 3a and 4a), though there is a new intense resonance at $g = 2.0$ with partially resolved ^{55}Mn hyperfine coupling. A close inspection of these resonances indicates that the partially resolved ^{55}Mn hyperfine coupling is most likely attributable to Mn(II) in the suprasil quartz EPR tubes. The presence of the new intense resonance suggests an equilibrium in which one or more of the ligands has dissociated from the manganese complex. In methanol (Figures S2b, S3, and S2d) ligand dissociation occurs to a greater extent as the EPR spectra reveal resonances from aquated Mn-(II).[51,52]

Generally Mn(II) EPR spectra are highly resolved with relatively narrow line widths which allows the observation of both ^{55}Mn and ligand hyperfine coupling. However, broad resonances in the solid and frozen solution EPR spectra have been reported for low symmetry ($E/D \neq 0$) mononuclear Mn-(II) complexes. For example, manganese complexes with penta- and hexadentate Schiff base ligands,[53] axially distorted Mn^{II}L$_4$X$_2$ complexes (L = pyridine and X = Br$^-$, Cl$^-$, I$^-$, or NCS$^-$), where D and E/D vary between 0.035 and 0.87 cm^{-1} and between 0.01 and 0.1 respectively,[54] Mn^{II}(Ph$_3$XO)$_4$Y$_2$ (X = P or As; Y = ClO$_4$, NCS, or I), where the average value of D is 0.18 cm^{-1} and E/D is 0.1,[55] the trigonal-bipyramidal complex [Mn^{II}(Me$_6$tren)X]X (X = Br or I; tren = 2,2′,2″-triaminotri-ethylamine) where D is 0.20 cm^{-1},[56] manganese(II) complexes with the general formula MnN$_4$X$_2$ (N = 4-methylpyridine,[57] pyrazine,[58,59] or hydrazine;[60] X = Br, Cl, or I) where D was found to increase in the order Cl < Br < I, and [Mn(sar)]$^{2+}$ (D = 0.19 cm^{-1} and E = 0.0063 cm^{-1}) and [Mn((NH$_3$)$_2$sar)]$^{4+}$ (D = 0.18 cm^{-1} and E = 0.012 cm^{-1}).[38] These examples suggest a qualitative relationship between site symmetry of the manganese center and the spectral line width. An increase in the distribution of D and E values may well explain the increase in spectral line width as the site symmetry is lowered.

Concluding Remarks

Interestingly, a comparison of the EPR parameters for the mononuclear [Mn([9]aneN$_2$S)$_2$](ClO$_4$)$_2$ and [Mn([9]aneN$_3$)$_2$]-(ClO$_4$)$_2$ complexes reveal that the manganese thioether complex has a larger axial distortion ($|D| = 0.19$ cm^{-1}) but smaller rhombic distortion ($E/D = 0.04$) than the hexaamine complex ($|D| = 0.09$ cm^{-1} and $E/D = 0.1$). The larger axial distortion for the manganese thioether complex is reflected in the X-ray crystallographic data which showed that the molecule was centrosymmetric with two long *trans* Mn−S bonds (2.625(3) Å). Both EPR and magnetic susceptibility data indicate that

(51) Hay, P. J.; Thibeault, J. C.; Hoffman, R. *J. Am. Chem. Soc.* **1975,** *97,* 4884.
(52) Blumberg, W. E. In *Magnetic Resonance in Biological Systems*; Ehrenberg, A., Malstrom, B. E., Vanngard, T., Eds.; Pergamon Press: London, 1967; p 119.
(53) Mabad, B.; Cassoux, P.; Tuchagues, J. -P.; Hendrickson, D. N. *Inorg. Chem.* **1986,** *25,* 1420.
(54) Slichter, C. P. *Principles of Magnetic Resonance*, 2nd ed., Springer-Verlag: Berlin, Heidelberg, Germany, **1978**.
(55) Goodgame, D. M. L.; Goodgame, M.; Hayward, P. J. *J. Chem. Soc. A* **1970**, 1352.
(56) Laskowski, E. J.; Hendrickson, D. N. *Inorg. Chem.* **1978,** *17,* 457.
(57) Birdy, R. B.; Goodgame, M. *J. Chem. Soc., Dalton Trans.* **1982,** 1429.
(58) Birdy, R. B.; Goodgame, M. *J. Chem. Soc., Dalton Trans.* **1983,** 1469.
(59) Kokoszka, G. F.; Duerst, R. W. *Coord. Chem. Rev.* **1970,** *5,* 209.
(60) Birdy, R. B.; Goodgame, M. *Inorg. Chim. Acta* **1981,** *50,* 183.

the $[Mn([9]aneN_2S)_2](ClO_4)_2$ and $[Mn([9]aneN_3)_2](ClO_4)_2$ complexes are high spin with an $S = {}^5/_2$ ground state.

Supporting Information Available: Table S1, containing complete crystal data for $[Mn([9]aneN_2S)_2](ClO_4)_2$, Table S2, containing thermal parameters ($\times 10^3$) for $[Mn([9]aneN_2S)_2](ClO_4)_2$, Table S3, containing hydrogen atom positional ($\times 10^3$) and thermal ($\times 10^2$) parameters for $[Mn([9]aneN_2S)_2](ClO_4)_2$, Figure S1, showing a variable temperature plot of the magnetic moment (μ_B) for $[Mn([9]aneN_2S)_2](ClO_4)_2$. Figure S2, showing frozen solution Q-band EPR spectra of (a) $[Mn([9]aneN_2S)_2](ClO_4)_2$ in acetonitrile−toluene (1:1), 130 K, $\nu = 34.0210$ GHz, (b) $[Mn([9]aneN_2S)_2](ClO_4)_2$ in methanol, 120 K, $\nu = 33.9218$ GHz, (c) $[Mn([9]aneN_3)_2](ClO_4)_2$ in acetonitrile−toluene (1:1), 120 K, an $\nu = 33.924$ GHz, and (d) $[Mn([9]aneN_2S)_2](ClO_4)_2$ in methanol, 120 K, $\nu = 33.9322$ GHz, and Figure S3, showing expansion of the EPR spectrum of $[Mn([9]aneN_2S)_2](ClO_4)_2$ (Figure S2) in methanol, 120 K, $\nu = 33.9322$ GHz (6 pages). Ordering information is given on any current masthead page.

IC950549C